AGU PUBLICATIONS

Geophysical Research Letters

RESEARCH LETTER
10.1002/2017GL074113

Key Points:
- Including gravity into elastic dislocation models significantly modifies the predicted displacement field
- The way in which gravity influences elastic displacement differs in the near-, medium-, and far-fields of the dislocation
- Far-field observations help to constrain slip inversions, especially when they are up-weighted relative to near-field observations

Supporting Information:
- Supporting Information S1

Correspondence to:
D. D. Gómez,
gomez.124@osu.edu

Citation:
Gómez, D. D., Bevis, M., Pan, E., & Smalley, R., Jr. (2017). The influence of gravity on the displacement field produced by fault slip. *Geophysical Research Letters*, *44*. https://doi.org/10.1002/2017GL074113

Received 10 MAY 2017
Accepted 6 SEP 2017
Accepted article online 11 SEP 2017

The Influence of Gravity on the Displacement Field Produced by Fault Slip

Demián D. Gómez[1,2], Michael Bevis[1], Ernian Pan[3], and Robert Smalley Jr.[4]

[1]School of Earth Sciences, Ohio State University, Columbus, OH, USA, [2]Instituto Geográfico Nacional, Buenos Aires, Argentina, [3]College of Engineering, University of Akron, Akron, OH, USA, [4]Center for Earthquake Research and Information, University of Memphis, Memphis, TN, USA

Abstract We calculated surface displacements produced by a synthetic megathrust earthquake using two spherical, layered, elastic dislocation models which differ only in that one model accounts for the coupling between elasticity and gravity and the other does not. We show that including gravity perturbs the displacement field differently in the near-, medium-, and far-fields. As a result, slip inversions based on an Earth model without gravity cannot simultaneously fit the near-, medium- and far-field displacements generated using a forward model including gravity. This suggests that the spatially systematic misfits between observations and dislocation predictions seen in the literature arise, at least in part, because these studies are based on models that neglect gravity. Although the magnitude of the far-field displacements is small compared to those of the near-field, our slip inversions show the most improvement when we both up-weight the far-field observations and use a physically consistent model in the inversion.

1. Introduction

Earthquakes have been modeled as dislocations embedded in an elastic medium for more than 50 years (Chinnery, 1961; Savage, 1980; Savage & Hastie, 1969; Steketee, 1958). Since the early 1990s most earthquake studies based on geodetic observations of coseismic displacements have used Okada's (1985) model of a rectangular dislocation embedded in a uniform elastic half-space. Okada's formalism is popular in part because it is very easy to use. But the Earth is neither uniform nor a half-space, and so there has been a steadily increasing interest in computing the deformation produced by more realistic models, such as dislocations in an anisotropic elastic half-space (Pan et al., 2014, 2015), a layered elastic half-space (Wang et al., 2003), or a layered elastic sphere (Pollitz, 1996; Sun et al., 2009). While the impact of layering and curvature is now well established (e.g., Sun & Okubo, 2002), there is relatively little consensus on the importance of including gravity into the Earth model. Even if we assume that the elastic deformation field caused by a given dislocation is not affected by gravity, that deformation does certainly modify the Earth's gravity field (Han et al., 2008; Heki & Matsuo, 2010) because it involves a redistribution of mass. Our concern here is more fundamental. For a given elastic Earth model, a specific fault geometry and specific slip distribution (Burgers vector field) on that dislocation, the final static deformation field produced by this dislocation must depend on the gravity field. This is because the final deformation field must minimize the total potential energy of the Earth, i.e., its gravitational potential energy plus its elastic strain energy, and not just its elastic strain energy. The question of practical interest is, what is the magnitude of the effect of gravity? Is the deformation produced by a given dislocation in a layered, spherical and self-gravitating elastic Earth significantly different from that predicted using a layered and spherical elastic Earth model without gravity?

Coupling between gravity and elasticity has been studied before (e.g., Rundle, 1980; Wang, 2005), but most publications mainly focused on the theory of the coupling between elasticity and gravity. Mysteriously, very few have sought to quantify this effect (e.g., Dong et al., 2014), even after it was suggested that near-field vertical uplift for a megathrust event might change by 20 cm when accounting for gravity (Wang, 2005). Moreover, following the analysis of Pollitz (1997), Segall (2010) concluded that the gravitational effects on coseismic deformation cannot be ignored for large magnitude earthquakes that generate displacements at distances of thousands of kilometers from the fault. To our knowledge, the effect of gravity on slip inversion and, in particular, the relative levels of error affecting the medium- and far-field displacements of megathrust earthquakes when we neglect gravity has not yet been studied in detail.

In this work, we address the importance of including gravity in the dislocation model. We use the finite element method (FEM) code *Pylith* (Aagaard et al., 2013), which can model the elastic dislocation problem in a layered, spherical Earth, both with and without gravity. Our analysis includes the displacement field in the area within approximately two fault dimensions (near-field), the area between two and five fault dimension (medium-field) and the area beyond five fault dimensions (far-field).

Prior to discussing *Pylith* and our analysis of the magnitude of the effect of including gravity in some detail, we offer some additional motivation for this study. We will show that the effect of gravity on dislocation-induced deformation is different in the near-, medium-, and far-fields of the dislocation. So if one inverts observed coseismic displacements by solving the forward problem using a model that ignores gravity, the model prediction errors will vary systematically with distance from the earthquake. As a result, the inferred slip distribution will be distorted, relative to the actual slip field, in order to drive agreement between the observed displacements and the systematically biased predictions of the forward model. Since short-term postseismic deformation is often modeled as afterslip on the same fault or plate boundary as the main event (Baba et al., 2006; Heki & Tamura, 1997; Perfettini et al., 2010), the same general problem will occur here also. Similarly, when interseismic deformation is modeled using Savage's (1983) virtual back slip formalism, the locking rate distribution may contain similar artifacts. There are increasing numbers of studies that examine the spatial relationship between coseismic slip, afterslip, and/or the interseismic locking rate (e.g., Moreno et al., 2010; Saillard et al., 2017), and there is a danger that such studies could be biased or distorted by the errors that arise when we neglect the effects of gravity.

2. Building and Validating a *Pylith* Model for a Megathrust Earthquake

For this synthetic study, we constructed a preliminary reference Earth model (Dziewonski & Anderson, 1981) based spherical, eight-layer FEM. The number of layers and their boundaries were selected to take into account jumps in V_p, V_s, and density so that these parameters can be adjusted using linear and step functions (see supporting information).

At the center of the domain, the FEM incorporates a shallow, planar thrust fault with dimensions 200 km (along strike) by 100 km (downdip) and a dip of 18° on which we applied up to 35 m of pure reverse slip. The slip applied to this fault varies systematically as a function of depth, from zero at the top of the fault at ~10 km depth, linearly increasing to a maximum of 35 m at ~20 km depth. At greater depths, slip decreases linearly with depth at half the previous rate of increase, so that at ~40 km depth the slip is again zero. There is no variation of slip along the strike of the fault. This slip distribution produces an earthquake of ~M_w 8.5.

We first validated the *Pylith* meshes by "turning gravity off" and comparing *Pylith*'s results for the near-, medium- and far-field displacements with those predicted by *Static1d* (Pollitz, 1996), which does not consider gravity, for the same fault geometry and slip distribution. We found the differences at all stations to be $<$0.8%. See the supporting information for a more detailed discussion of this validation study.

To incorporate gravity, *Pylith* uses the total Lagrangian formulation based on that of Bathe (1995) which includes gravity as a body force (*Pylith* Manual, Aagaard et al., 2017) pointing toward the geocenter (with a force per unit volume equal to the density times the gravity acceleration). When a gravity field is invoked, it is necessary to specify a consistent distribution of lithostatic stress within the mesh before running the program, so that the FEM achieves static equilibrium (*Pylith* Manual, Aagaard et al. (2017)).

Following Pollitz (1997) and Segall (2010), the gravitational effects on elastic deformation can be separated into "little g" and "big G" terms. *Pylith*'s handling of gravity is approximate because it only includes the effect of little g and ignores the big G gravitational term. Although both terms have significant effects at distances of thousands of km from the fault, little g is the dominant effect by almost an order of magnitude at distances of ~1,000 km (Segall, 2010). Therefore, the errors precipitated by the approximations made in *Pylith* are much smaller than those induced by neglecting gravity altogether (as done by other open source codes). Also, *Pylith* assumes that the magnitude of the acceleration due to gravity, g, is constant throughout the model. However, when we model just the upper mantle and lithosphere (Figure S1a), this is a very good approximation (Figure S2b).

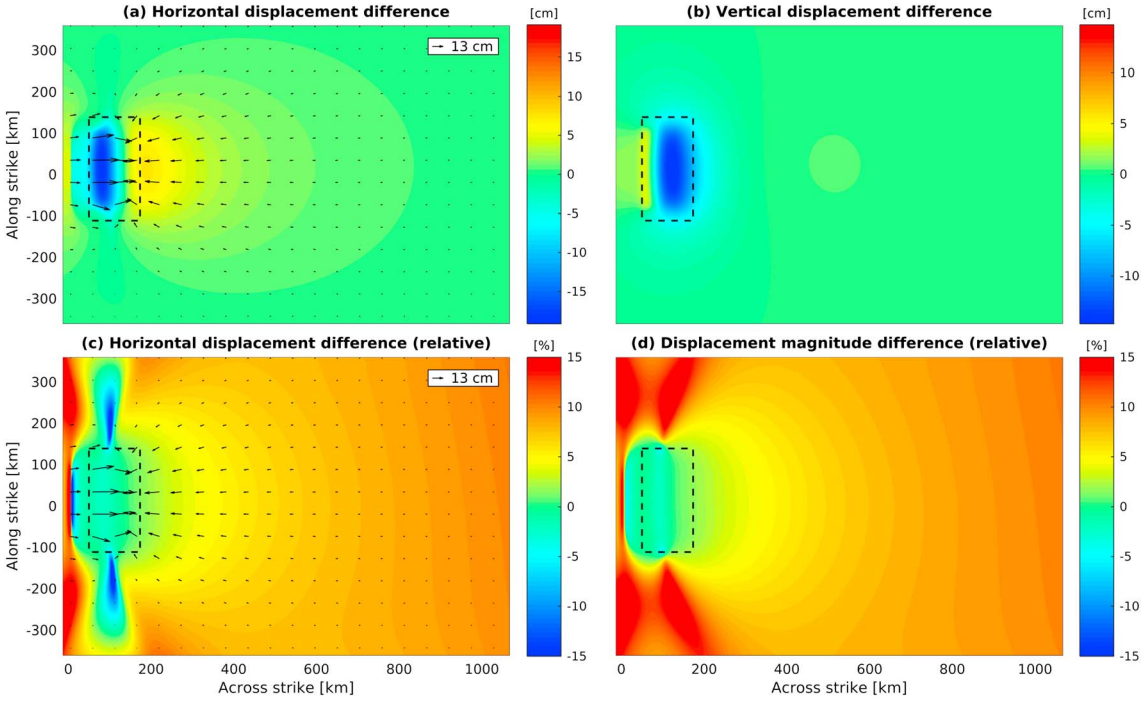

Figure 1. (a) Absolute horizontal surface displacement difference between models with gravity and without gravity. Vectors show the relative displacement difference. Black dashed line shows the location of slip. (b) Same as Figure 1a for the vertical component. (c) Same as Figure 1a normalized by the without gravity magnitude. Vectors as in Figure 1a. (d) Normalized total displacement magnitude difference.

3. The Impact of Gravity on the Displacements Produced by a Megathrust Event

To show the discrepancy between models including and neglecting gravity, we estimated the elastic surface displacements using *Pylith* for two models: one with gravity (WG) and another one without gravity (WoG). Figure 1a shows the absolute horizontal surface displacement field difference between WG and WoG as a contour plot and vector field. Notice that the majority of the horizontal difference is located near the rupture zone and in the direction of increasing distance across strike. In the vertical direction (Figure 1b), the majority of the difference is also located within the rupture zone.

The difference between models relative to WoG displacements (Figure 1c) shows horizontal discrepancies between −15 and 15%, where one can see that the relative differences become larger toward the far-field. Analyzing the relative differences of magnitude of the total displacement (Figure 1d), we note that toward the far-field the discrepancy reaches ~8%, while in the regions along strike from the rupture zone the discrepancy is as large as ~15%.

Although the largest absolute displacement differences due to gravity occurred near the rupture zone, Figure 1d shows that the near-field relative differences were approximately uniform, never exceeding ~−4%. In the medium-field, past 400 km from the trench toward the far-field, however, these discrepancies had a positive sign, reaching up to 10% within 1,000 km from the rupture zone. This indicates that gravity introduces a relative discrepancy between the near and far-fields of up to 14%. Along strike from the rupture zone, as in the far-field, the absolute differences were small, but the relative differences reached up to 15% (positive). Therefore, the peak-to-peak relative difference between the regions along strike and the rupture zone is ~20%.

Previous studies indicated that the discrepancies due to neglecting the effect of gravity in the near-field do not have a large impact on the slip distribution (Pollitz, 1996). This is confirmed by our observations, since within the near-field, the discrepancies between models were low and uniformly bounded to no more than 4%. However, the effect on slip inversion of the differing displacement perturbations in the near-, medium-, and far-field has never been quantified. Next, we studied the effect of neglecting gravity on the slip inversion problem.

4. Far-Field Observations Improve the Slip Estimated by the Inversion

We will show that up-weighting far-field observations improve the slip estimation on the fault. To simulate the observation conditions of a real earthquake, we used a set of ~150 GPS sites inspired by the observation geometries in South America. We obtained the influence matrices (IMs) or impulse responses of each fault node of WoG at a set of stations distributed from the approximate position of the coastline (near-field) to about 1,400 km from the trench (far-field). To emphasize the effect of gravity, we only consider dip slip, which has the largest effect, rather than both dip slip and strike slip, since incorporating another variable to the inverse problem requires setting up additional constraints that would obscure the point we wish to emphasize.

Our inversion strategy incorporated a numerical implementation of the Laplacian operator known as the scale-dependent umbrella operator (Maerten et al., 2005) to help constrain and smooth the solution. We also used constrained least squares and assumed limits for the magnitude of slip. This is a very common practice used to constrain the slip based on previous knowledge about the fault.

We will show the results from two observation weighting schemes, one that assigns uniform weights based on the estimated uncertainties of GPS coseismic observations, which are ~2 mm in the horizontal and ~5 mm in the vertical component (hereafter UW) and another one that uses heterogeneous weights (HW) which takes into account both the uncertainty and the influence of each station in the inversion (i.e., the values of the IMs). The expression used for HW and the validation of our inverse method using noiseless data can be found in the supporting information.

Although the error distribution in GPS time series is unknown, we applied random white noise to the synthetic displacement field in order to simulate the uncertainty of GPS-observed coseismic displacements. To avoid using observations with low signal-to-noise ratio (SNR), we discarded the displacements with SNR < 10. This is a quite conservative threshold that guarantees that the up-weighted inversion will not be affected by the lower SNR in the far-field.

Figure 2a shows the "true" slip distribution used to calculate the synthetic displacement field; in this case WoG, Figure 2b shows the estimated slip distribution and Figure 2c the difference between the forward and estimated slip distributions. For this inversion, we used UW and moderate smoothing ($s = 0.2$) which yields the best compromise between smoothing and surface displacement misfit. We notice two dominant regions of slip with slip deficiency between them (between ~40 and 50 km along strike) created by the resolution of the stations' distribution. We computed an RMS misfit of ~4 m between the "true" and that estimated slip. This value represents the overall misfit created by the artifacts observed in the profile shown in Figure 2d. We also calculated the sum of the misfits of the surface displacements relative to the maximum displacement magnitude to illustrate, using a single value, the level of agreement between the forward (noiseless) and the modeled displacements. Although the agreement between the "true" and estimated slip is poor, the surface displacement misfit is ~1% with maximum misfit reaching 5% (Figure 2e). The effect introduced by smoothing the slip is visible in the profile shown in Figure 2d, where we observe smoothing of sharp changes in the slip distribution. Although such discontinuities in slip are unrealistic, we allowed them to quantify effects like the one we describe here.

We inverted for the slip distribution a second time with the same smoothing, but now using HW. The results are shown in Figures 3a–3e, where we notice that increasing the weight of the far-field observations helps to better constrain the solution. The magnitude of the artifacts observed in Figure 2c was significantly reduced, with an RMS misfit of the slip distribution of 2 m. The total surface displacement misfit decreased down to ~0.7% and the maximum misfit is now ~1.2%. We performed several inversions to analyze the variability of the results due to changes in the random noise and in all cases HW showed a misfit improvement. Our analysis showed that the slip misfit varies by ~±0.5 m and that the surface displacement misfit can vary as much as ±0.7%. For all cases, we noticed a tendency of HW to distribute the misfit more evenly among observations, while UW tends to localize the misfit in the regions along strike from the rupture zone, at stations with low IM. This effect was also observed during the noiseless tests (see supporting information).

The improvement from UW to HW can be explained by the nature of the far-field sensitivity to the slip at the fault. Far-field observations are not sensitive to the short wavelengths of slip distribution but are sensitive to the depth of the slip. Therefore, medium- and far-field stations have poor resolution but they can be used to

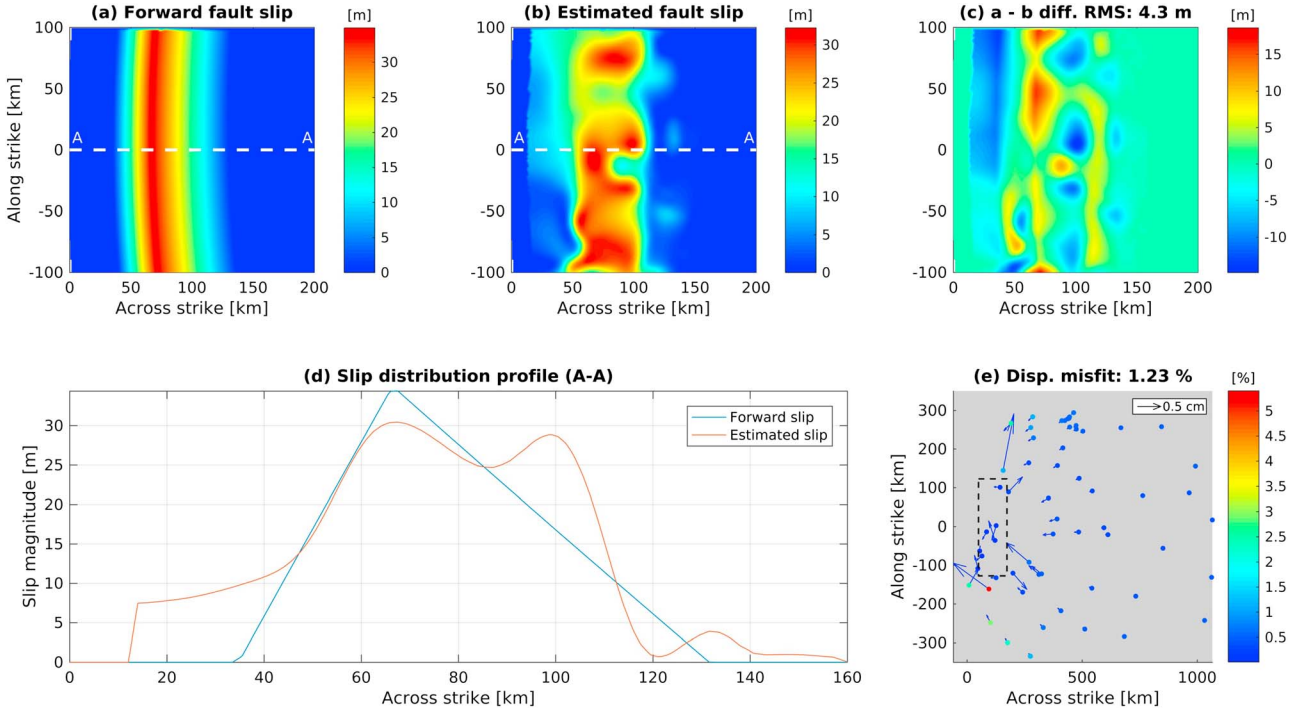

Figure 2. (a) Forward imposed fault slip for the model without gravity. White dashed line shows location of the profile in part d. (b) Slip estimated from inversion using the influence matrices of the model without gravity and the uncertainty weighing scheme. (c) Difference between forward imposed and estimated slip. (d) Profile of the forward and estimated slip distributions. (e) Surface displacement misfits relative to the forward displacements (noiseless) and vector field showing the absolute misfit. Most of the misfit is located in the along strike direction from the fault with a total misfit (sum of the misfits normalized by the largest displacement) of ~1%.

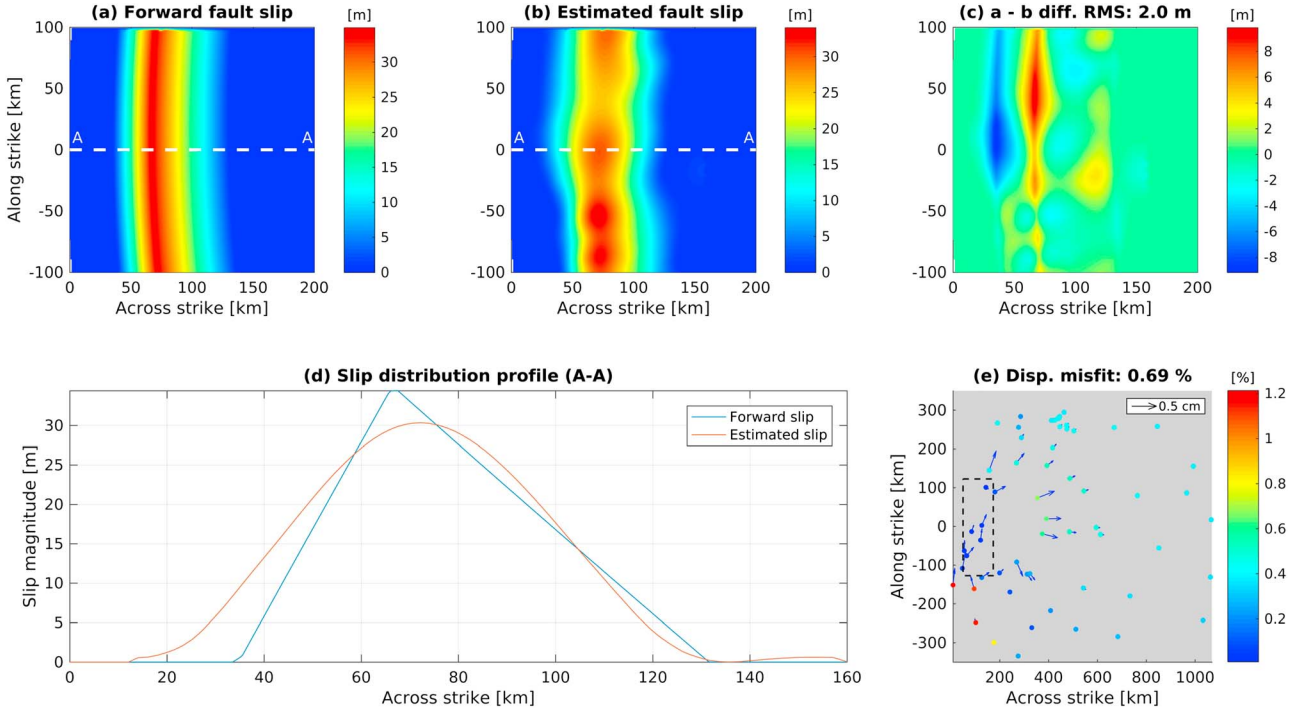

Figure 3. Same as Figure 2 but using the heterogeneous weighing scheme. The artifacts in part c were significantly reduced to almost half of the amplitude of those in Figure 2. The RMS misfit of this inversion was 2 m. Also, the misfits in part e are more evenly distributed among observations compared to those in Figure 2e.

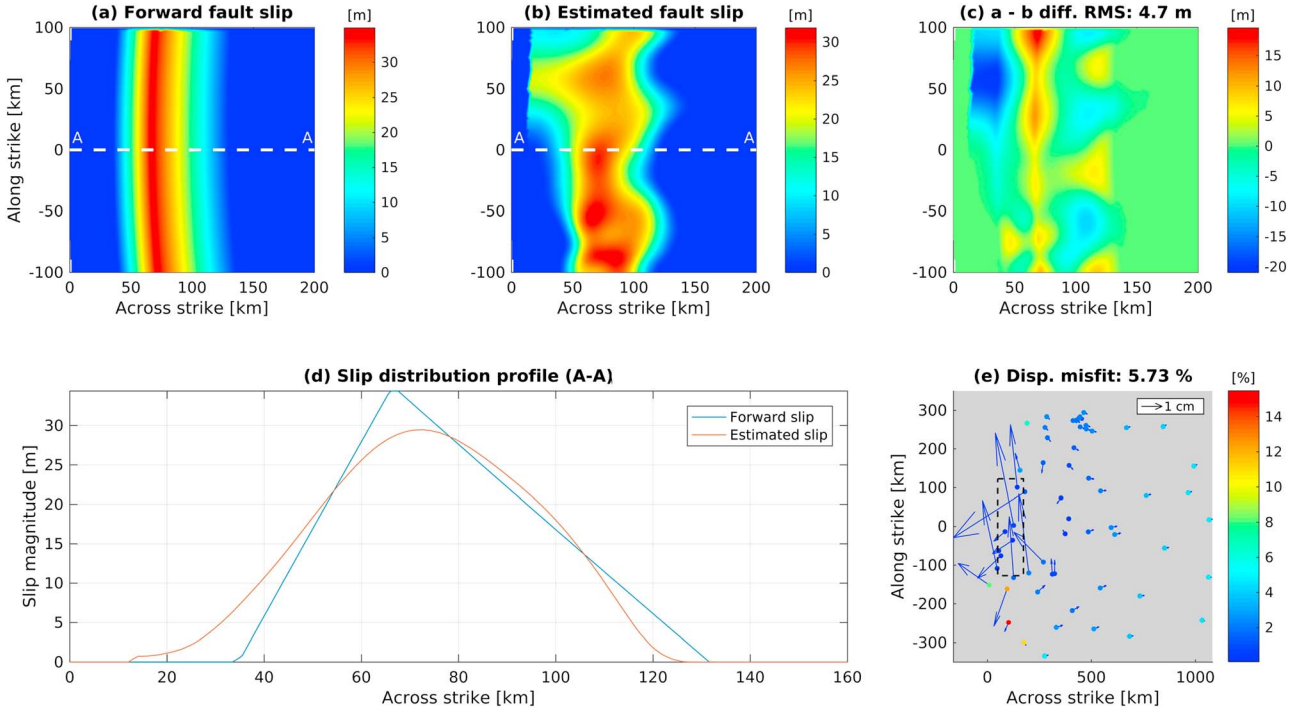

Figure 4. Estimated slip obtained by using the forward displacements of the model calculated with gravity and the influence matrices of the model without gravity, and the heterogeneous weighing scheme.

constrain the long wavelengths of the slip distribution when there are gaps in the near-field station coverage. Contrary to the common practice of neglecting far-field displacements during slip inversion, this test shows that the information contained in the far-field observations can be useful to constrain the slip on the fault.

5. The Effect of Neglecting Gravity During Slip Inversion

In this section we will address the inconsistencies found during slip inversion using a dislocation model that does not take gravity into account. We replicate the most common practice in earthquake deformation analysis, inverting for the slip distribution that occurs in a real-world WG, using a model WoG for the IMs in the inversion (hereafter WG-WoG). Our first attempt was to use the same smoothing parameter and weighting scheme that provided the best results in the previous section (moderate smoothing and HW). This, however, results in a WG-WoG slip distribution that contains large artifacts. This effect is due to the weighing scheme and the trade-off between the near-, medium-, and the far-field displacements introduced by gravity; thus, we cannot fit the near-, medium-, and the far-field observations simultaneously (see supporting information).

To mitigate this issue, there are at least two options: (1) use UW rather than HW or (2) increase the level of smoothing. In this section we did not use UW, since our goal is to obtain a slip distribution that fits the near-, medium-, and the far-field displacements simultaneously. Although other least squares techniques could be used to stabilize the inverse problem, these methods are beyond the scope of this work.

We therefore focused on estimating the best smoothing or regularization parameter for the inversion. This parameter controls the trade-off between the roughness of the solution and the surface displacement misfit. For a real earthquake, the most common practice to choose the smoothing parameter is to plot the misfit as a function of smoothing and select its value so that the misfit is about the noise level of the data. This method provides the best procedure to reach a compromise value of smoothing that guarantees the minimum misfit.

In this study, we want to show that even when selecting the best possible smoothing parameter the WG-WoG solution is still worse than that found when using a consistent Earth model. To do this, we selected the best smoothing parameter based on the misfit of both the slip and the resulting displacement field. This procedure is not applicable to real data since the actual slip distribution is unknown. Nevertheless, this will show

that even the best WG-WoG estimation is unable to match that using consistent IMs. We found a compromise smoothing value of $s = 0.3$, (see Figure S6) which is 50% larger than the value used during the inversion using WoG displacements. Figures 4a–4e show that the solution exhibits large artifacts necessary to fit the surface deformation. Those artifacts reached almost 50% of the forward slip maximum amplitude, with an RMS misfit of ~5 m. The total misfit of this inverse solution is ~6%.

The weighting scheme should still have favored a lower misfit in the far-field and anywhere with low response to fault slip. Figure 4e shows, however, that the misfit in the far-field and in the regions along strike of the rupture zone is between 5 and 14%. Therefore, this fit was obtained by allowing larger absolute misfits in the medium- and far-fields.

6. Discussion and Conclusions

Most elastic dislocation models of great megathrust earthquakes (which generate observable surface displacements more than several fault dimensions away from the rupture zone) can be divided into two classes: those that ignore the far-field observations and only focus on the near-field deformation to infer the slip distribution (e.g., Delouis et al., 2010; Tong et al., 2010) and those that model both near-field and far-field deformation but are plagued by spatially systematic disagreements between the predicted and observed displacements (Pollitz et al., 2011).

Most articles that restrict their attention to near-field observations use Okada's homogeneous half-space model, which is an inappropriate framework for modeling coseismic displacements on a layered and nearly spherical Earth. Researchers who adopt Okada's formulation often justify this choice by claiming that when modeling displacements at GPS stations close to the rupture zone, neglecting layering, sphericity, and gravity will have little impact on the estimated slip distribution. Even if this were true, their final slip model would not correctly predict observed far-field displacements, and simply excluding such observations from their analysis in no way alleviates this deficiency. It simply ignores it.

The issue of sphericity and layering has already been addressed by others, but until now, the effect of gravity on slip inversions has not been described in detail. We have shown that including gravity can generate displacement differences of almost 15% in the near-field and close to the edges along strike of the rupture zone. Therefore, any dislocation model that does not account for gravity will produce a distorted, or biased, inversion for slip even when the inversion is limited to observations of displacement in and around the rupture zone.

Many studies of coseismic displacements that invert all available displacement data using Okada's model or the layered elastic half-space model of Wang et al. (2003) (e.g., Lin et al., 2013; Vigny et al., 2011) cannot fit both the near- and far-field observations, at least if they insist on a reasonably smooth distribution of fault slip. The problem hidden in analyses restricted to the near-field data is now revealed. It is possible to mitigate this misfit problem by brute force, by introducing very large numbers of degrees of freedom into the slip field, but only at the cost of producing implausibly complicated slip distributions. It is widely understood that if the number of adjustable model parameters almost equals the number of observations, good agreement between the observed and calculated values is little more than a tautology and is physically unconvincing. The misfit problem tends to be most apparent in Okada-based inversions because the impact of layering, sphericity, and gravity are *all* neglected. But we have shown that even when sphericity and layering are accounted for, incorporating gravity significantly perturbs the predicted surface displacement fields at nearly all distances and that the character of these perturbations differ in the near-, medium-, and far-fields. As a result, ignoring the gravity effect necessarily distorts the inferred distribution of slip.

We conclude that realistic static displacement predictions and slip solutions for great megathrust earthquakes can be achieved only if we account for gravity as well as for sphericity and layering. The gravity effect is especially important in subduction zone environments such as the South America-Nazca plate boundary where deformations generated by the recent megathrust earthquakes can be measured across the whole of South America, from the Pacific to the Atlantic coastlines. Perhaps because the gravity effect varies with distance from the rupture zone, judicious up-weighting of far-field observations can lead to better solutions for the slip distribution. The Central Andes GPS Project group is currently working to

produce a realistic FEM that incorporates gravity to model the displacement field of recent events such as the 2010 M_w 8.8 Maule earthquake.

Acknowledgments
This work was supported by the NSF awards EAR-1118241 and EAR-1118514. We thank the Computational Infrastructure for Geodynamics (geodynamics.org) which is funded by the National Science Foundation under award NSF-0949446. We would also like to thank Paul Segall and an anonymous reviewer for their very insightful comments and suggestions that led to significant improvements in the manuscript.

References

Aagaard, B. T., Knepley, M. G., & Williams, C. A. (2013). A domain decomposition approach to implementing fault slip in finite-element models of quasi-static and dynamic crustal deformation. *Journal of Geophysical Research: Solid Earth*, *118*(6), 3059–3079. https://doi.org/10.1002/jgrb.50217

Aagaard, B. T., Knepley, M. G., & Williams, C. A. (2017). PyLith v2.2.0, Davis CA. *Computational Infrastructure for Geodynamics*. https://doi.org/10.5281/zenodo.438705

Baba, T., Hirata, K., Hori, T., & Sakaguchi, H. (2006). Offshore geodetic data conducive to the estimation of the afterslip distribution following the 2003 Tokachi-oki earthquake. *Earth and Planetary Science Letters*, *241*(1–2), 281–292. https://doi.org/10.1016/j.epsl.2005.10.019

Bathe, K. J. (1995). *Finite element procedures*. Upper Saddle River, NJ: Prentice Hall.

Chinnery, M. A. (1961). The deformation of the ground around surface faults. *Bulletin of the Seismological Society of America*, *51*(3), 355–372.

Delouis, B., Nocquet, J.-M., & Vallée, M. (2010). Slip distribution of the February 27, 2010 M_w = 8.8 Maule Earthquake, central Chile, from static and high-rate GPS, InSAR, and broadband teleseismic data. *Geophysical Research Letters*, *37*, L17305. https://doi.org/10.1029/2010GL043899

Dong, J., Sun, W., Zhou, X., & Wang, R. (2014). Effects of Earth's layered structure, gravity and curvature on coseismic deformation. *Geophysical Journal International*, *199*(3), 1442–1451. https://doi.org/10.1093/gji/ggu342

Dziewonski, A. M., & Anderson, D. L. (1981). Preliminary reference Earth model. *Physics of the Earth and Planetary Interiors*, *25*(4), 297–356.

Han, S.-C., Sauber, J., Luthcke, S. B., Ji, C., & Pollitz, F. F. (2008). Implications of postseismic gravity change following the great 2004 Sumatra-Andaman earthquake from the regional harmonic analysis of GRACE intersatellite tracking data. *Journal of Geophysical Research*, *113*, B11413. https://doi.org/10.1029/2008JB005705

Heki, K., & Matsuo, K. (2010). Coseismic gravity changes of the 2010 earthquake in central Chile from satellite gravimetry. *Geophysical Research Letters*, *37*, L24306. https://doi.org/10.1029/2010GL045335

Heki, K., & Tamura, Y. (1997). Short term afterslip in the 1994 Sanriku-Haruka-Oki Earthquake. *Geophysical Research Letters*, *24*(24), 3285–3288. https://doi.org/10.1029/97GL03316

Lin, Y. N., Sladen, A., Ortega-Culaciati, F., Simons, M., Avouac, J.-P., Fielding, E. J., … Socquet, A. (2013). Coseismic and postseismic slip associated with the 2010 Maule Earthquake, Chile: Characterizing the Arauco Peninsula barrier effect. *Journal of Geophysical Research: Solid Earth*, *118*, 3142–3159. https://doi.org/10.1002/jgrb.50207

Maerten, F., Resor, P., Polland, D., & Maerten, L. (2005). Inverting for slip on three-dimensional fault surfaces using angular dislocations. *Bulletin of the Seismological Society of America*, *95*(5), 1654–1665. https://doi.org/10.1785/0120030181

Moreno, M., Rosenau, M., & Oncken, O. (2010). 2010 Maule earthquake slip correlates with pre-seismic locking of Andean subduction zone. *Nature*, *467*(7312), 198–202.

Okada, Y. (1985). Surface deformation due to shear and tensile faults in a half-space. *Bulletin of the Seismological Society of America*, *75*(4), 1135–1154.

Pan, E., Yuan, J. H., Chen, W. Q., & Griffith, W. A. (2014). Elastic deformation due to polygonal dislocations in a transversely isotropic half-space. *Bulletin of the Seismological Society of America*, *104*(6), 2698–2716.

Pan, E., Tabrizi, A. M., Sangghaleh, A., & Griffith, W. A. (2015). Displacement and stress fields due to finite faults and opening-mode fractures in an anisotropic elastic half-space. *Geophysical Journal International*, *203*(2), 1193–1206.

Perfettini, H., et al. (2010). Seismic and aseismic slip on the Central Peru megathrust. *Nature*, *465*(7294), 78–81. https://doi.org/10.1038/nature09062

Pollitz, F. F. (1996). Coseismic deformation from earthquake faulting on a layered spherical Earth. *Geophysical Journal International*, *125*(1), 1–14.

Pollitz, F. F. (1997). Gravitational viscoelastic postseismic relaxation on a layered spherical Earth. *Journal of Geophysical Research*, *102*(B8), 17921–17941. https://doi.org/10.1029/97JB01277

Pollitz, F. F., Brooks, B., Tong, X., Bevis, M. G., Foster, J. H., Bűrgmann, R., … Blanco, M. (2011). Coseismic slip distribution of the February 27, 2010 M_w 8.8 Maule, Chile earthquake. *Geophysical Research Letters*, *38*, L09309. https://doi.org/10.1029/2011GL047065

Rundle, J. B. (1980). Static elastic-gravitational deformation of a layered half space by point couple sources. *Journal of Geophysical Research*, *85*(B10), 5355–5363. https://doi.org/10.1029/JB085iB10p05355

Saillard, M., Audin, L., Rousset, B., Avouac, J.-P., Chlieh, M., Hall, S. R., … Farber, D. L. (2017). From the seismic cycle to long-term deformation: Linking seismic coupling and Quaternary coastal geomorphology along the Andean megathrust. *Tectonics*, *36*, 241–256. https://doi.org/10.1002/2016TC004156

Savage, J. C. (1980). Dislocations in seismology. In F. R. N. Navarro (Ed.), *Dislocations in solids*, *moving dislocations* (Vol. 3, pp. 252–339). Amsterdam.

Savage, J. C. (1983). A dislocation model of strain accumulation and release at a subduction zone. *Journal of Geophysical Research*, *88*(6), 4984–4996.

Savage, J. C., & Hastie, L. M. (1969). A dislocation model for the Fairview Peak, Nevada, earthquake. *Bulletin of the Seismological Society of America*, *59*(5), 1937–1948.

Segall, P. (2010). *Earthquake and volcano deformation*. Princeton, NJ: Princeton Univ. Press.

Steketee, J. A. (1958). On Volterra's dislocations in a semi-infinite elastic medium. *Canadian Journal of Physics*, *36*(2), 192–205. https://doi.org/10.1139/p58-024

Sun, W., & Okubo, S. (2002). Effects of earth's spherical curvature and radial heterogeneity in dislocation studies—for a point dislocation. *Geophysical Research Letters*, *29*(12), 46–41. https://doi.org/10.1029/2001GL014497

Sun, W., Okubo, S., Fu, G., & Araya, A. (2009). General formulations of global co-seismic deformations caused by an arbitrary dislocation in a spherically symmetric earth model-applicable to deformed earth surface and space-fixed point. *Geophysical Journal International*, *177*(3), 817–833. https://doi.org/10.1111/j.1365-246X.2009.04113.x

Tong, X., Sandwell, D., Luttrell, K., Brooks, B., Bevis, M., Shimada, M., … Caccamise, D. J., II (2010). The 2010 Maule, Chile earthquake: Downdip rupture limit revealed by space geodesy. *Geophysical Research Letters*, *37*, L24311. https://doi.org/10.1029/2010GL045805

Vigny, C., Socquet, A., Peyrat, S., Ruegg, J.-C., Métois, M., Madariaga, R., … Kendrick, E. (2011). The 2010 M_w 8.8 Maule megathrust earthquake of central Chile, monitored by GPS. *Science*, *332*(6036), 1417–1421. https://doi.org/10.1126/science.1204132

Wang, R. (2005). The dislocation theory: A consistent way for including the gravity effect in (visco)elastic plane-earth models. *Geophysical Journal International*, *161*(1), 191–196. https://doi.org/10.1111/j.1365-246X.2005.02614.x

Wang, R., Martín, F. L., & Roth, F. (2003). Computation of deformation induced by earthquakes in a multi-layered elastic crust—FORTRAN programs EDGRN/EDCMP. *Computational Geosciences*, *29*(2), 195–207.